ISSN 1674-1056
http://cpb.iphy.ac.cn
http://iopscience.iop.org/cpb
中国物理 B
Chinese Physics
中国物理
Chinese Physics B

Flow characteristics of supersonic gas passing through circular micro-channel under different inflow conditions

Guang-Ming Guo(郭广明), Qin Luo(罗琴), Lin Zhu(朱林), Yi-Xiang Bian(边义祥)

Citation: Chin. Phys. B . 2019, 28(6): 064702. **doi:** 10.1088/1674-1056/28/6/064702
Journal homepage: http://cpb.iphy.ac.cn; http://iopscience.iop.org/cpb

What follows is a list of articles you may be interested in

Aerodynamic measurement of a large aircraft modelin hypersonic flow

Bao-Qing Meng(孟宝清), Gui-Lai Han(韩桂来), De-Liang Zhang(张德良), Zong-Lin Jiang(姜宗林)

Chin. Phys. B . 2017, 26(11): 114702. **doi:** 10.1088/1674-1056/26/11/114702

Development of a new correlation to calculate permeability for flows with high Knudsen number

Esmaeil Dehdashti

Chin. Phys. B . 2016, 25(2): 024702. **doi:** 10.1088/1674-1056/25/2/024702

Multi-relaxation time lattice Boltzmann simulation of inertial secondary flow in a curved microchannel

Sun Dong-Ke, Xiang Nan, Jiang Di, Chen Ke, Yi Hong, Ni Zhong-Hua

Chin. Phys. B . 2013, 22(11): 114704. **doi:** 10.1088/1674-1056/22/11/114704

Simultaneous density and velocity measurements in a supersonic turbulent boundary layer

He Lin, Yi Shi-He, Tian Li-Feng, Chen Zhi, Zhu Yang-Zhu

Chin. Phys. B . 2013, 22(2): 024704. **doi:** 10.1088/1674-1056/22/2/024704

Instantaneous and time-averaged flow structures around a blunt double-cone with or without supersonic film cooling visualized via nano-tracer planar laser scattering

Zhu Yang-Zhu, Yi Shi-He, He Lin, Tian Li-Feng, Zhou Yong-Wei

Chin. Phys. B . 2013, 22(1): 014702. **doi:** 10.1088/1674-1056/22/1/014702

Flow characteristics of supersonic gas passing through a circular micro-channel under different inflow conditions*

Guang-Ming Guo(郭广明)[1,†], Qin Luo(罗琴)[2], Lin Zhu(朱林)[1], and Yi-Xiang Bian(边义祥)[1]

[1] College of Mechanical Engineering, Yangzhou University, Yangzhou 225127, China
[2] College of Information Engineering, Yangzhou University, Yangzhou 225127, China

(Received 21 January 2019; revised manuscript received 21 February 2019; published online 8 May 2019)

Gas flow in a micro-channel usually has a high Knudsen number. The predominant predictive tool for such a micro-flow is the direct simulation Monte Carlo (DSMC) method, which is used in this paper to investigate primary flow properties of supersonic gas in a circular micro-channel for different inflow conditions, such as free stream at different altitudes, with different incoming Mach numbers, and with different angles of attack. Simulation results indicate that the altitude and free stream incoming Mach number have a significant effect on the whole micro-channel flow field, whereas the angle of attack mainly affects the entrance part of micro-channel flow field. The fundamental mechanism behind the simulation results is also presented. With the increase of altitude, thr free stream would be partly prevented from entering into micro-channel. Meanwhile, the gas flow in micro-channel is decelerated, and the increase in the angle of attack also decelerates the gas flow. In contrast, gas flow in micro-channel is accelerated as free stream incoming Mach number increases. A noteworthy finding is that the rarefaction effects can become very dominant when the free stream incoming Mach number is low. In other words, a free stream with a larger incoming velocity is able to reduce the influence of the rarefaction effects on gas flow in the micro-channel.

Keywords: rarefied flow, micro-channel, mass flow velocity, temperature distribution

PACS: 47.27.nd, 47.40.Ki, 47.11.Mn, 47.45.–n **DOI:** 10.1088/1674-1056/28/6/064702

1. Introduction

With the great progress of manufacturing technologies, such as silicon micro machining, optical lithography, etching and electrical discharge machining, micro-electro-mechanical system (MEMS) has become an emerging field with great growth prospects.[1,2] Microsystems based on the MEMS are capable of sensing and controlling physical processes on a scale of length on the order of one micron, or even sub-micron.[3] Current applications for such micro devices include thermo-mechanical data storage, high temperature pressure sensor, micro-nozzle, micro-sensor, and micro-pump, *etc*. Despite the growing applications of MEMS in scientific and engineering devices, the understanding of its fluid dynamics is far from satisfactory degree.[4] Because the MEMS includes many micro-channels and in most cases, the micro-channel height is comparable to the mean free path of gas molecules, the performance of MEMS often does not conform to the predictions made by using scaling laws developed for macro-scale systems. The gas in the micro-channel is rather rarefied[5] and such a micro-flow should be simulated by the methods developed for the micro-scale systems.

According to the Knudsen number Kn (a dimensionless number indicating the rarefied degree of flow and it is the ratio of mean free path of gas molecule to the micro-channel diameter in this study. The bigger the Knudsen number, the more rarefied the gas is), the gas flow in the micro-channel is usually in the transition regime.[6] Consequently, the traditional CFD techniques based on continuum hypothesis of fluids may lead to large errors when they are used to analyze micro-channel flow. To accurately analyze the rarefied gas flows, the approaches based on the solution of the Boltzmann equation must be adopted.[7] As one of the most successful particle simulation methods of treating rarefied gas flows,[8] the direct simulation Monte Carlo (DSMC) method first proposed by Bird is capable of solving the Boltzmann equation based on direct statistical simulation of the molecular process described by kinetic theory.[9,10] Therefore, the gas flow in a micro-channel can be described by using the DSMC method and it has been widely applied to the prediction of rarefied gas flows.

In micro-channel numerical simulations, most researchers have focused on the flow field in the micro-channels.[11–16] Taheri and Struchtrup[17] investigated the flow structure in a parallel plate micro-channel, where a streamwise constant temperature gradient is applied in the channel walls, and typical non-equilibrium effects at the boundary are investigated by solving the regularized 13-moment equations. The DSMC simulations were carried out of gas flows for varying degrees of rarefaction along micro-channels with both one and two 90-degree bends by White *et al.*[18] and it was shown that

*Project supported by the National Natural Science Foundation of China (Grant No. 11802264) and the Natural Science Foundation of Jiangsu Province, China (Grant No. BK20180896).

†Corresponding author. E-mail: guoming20071028@163.com

© 2019 Chinese Physical Society and IOP Publishing Ltd

the choice of mesh size in the corner region is important for capturing the size and shape of any recirculation region. Darbandi and Roohi[5] simulated a subsonic flow in nanochannels and adopted the micro/nanoscale backward-facing steps by the DSMC method. They observed that the pressure distribution along the channel deviates from a linear distribution as soon as the Knudsen number reaches the early free-molecular regime and the length of separation region considerably decreases as the flow influences more in the transition regime region. Zhen *et al.*[19] employed the DSMC method and analyzed the rationality of the two-dimensional (2D) simplification for a three-dimensional (3D) straight rectangular cross-sectional micro-channel. The calculated flow properties in the 3D case are compared with the results of the 2D case and the authors found that the 2D simplification is reasonable when the cross aspect ratio is greater than 5. Gatsonis *et al.*[20] used an unstructured DSMC solver and simulated supersonic flow in 3D nanochannels, and physical aspects of supersonic flows in nanoscale rectangular channels were revealed. Ejtehadi *et al.*[21] simulated a rarefied gas flow between two parallel moving micro-plates maintained at the same uniform temperature by the DSMC method and influences of important molecular structural parameters, such as molecular diameter, mass, degrees of freedom, and viscosity–temperature index on the macroscopic behaviors of the rarefied gas flow (*e.g.*, velocity, temperature, heat flux and shear stress coefficients) were investigated. Liou and Fang[22] investigated the heat transfer characteristics and velocity in a 2D micro-channel by the DSMC method. Their results showed that the heat transfer characteristics of the micro-channel flow can vary significantly with the Knudsen number of the incoming flow and the enhanced wall heat transfer is mainly caused by increasing the number rate of molecules that impact the wall.

As reviewed above, micro-channel flows have been investigated from many different aspects by many researchers. However, to the best of the authors' knowledge, the influence of altitude and free stream inflow direction on the flow of gas in the micro-channel have not yet been investigated. Actually, micro-channels in practical applications tend to have different altitudes and the free stream inflow direction is also variable, so there is a clear need for DSMC data about the effect that is exerted on the micro-channel gas flow by the altitude and the free stream inflow direction. Moreover, the free stream with supersonic speed should be taken into account to explore flow characteristics of the high-speed gas in the micro-channel to understand the problem of micro-channel flow in depth. Therefore, motivated by the lack of such results, this study investigates the variable parameters, such as altitude, free stream inflow direction, and incoming Mach number, to explore their effects on flow properties of supersonic gas in the micro-channel.

The rest of this paper is organized as follows. The DSMC method is briefly introduced and validated in Section 2. In Section 3, the DSMC simulation cases are described in detail. The results of the DSMC simulations and discussion are given in Section 4. Finally, the significant conclusions are drawn from the present study in Section 5.

2. DSMC method and code validation

2.1. DSMC introduction

According to Refs. [9] and [10] the Boltzmann equation is able to describe the flow behaviors of gas at each rarefaction degree[23] and it can be solved by stochastic schemes, commonly known as DSMC. In short, the DSMC method is a particle based microscopic method that converges to the solution of the Boltzmann equation in the limit of infinite simulating particles.[10] In this method, simulating particles represent a cloud of gas molecules that travel and collide with each other and solid surfaces. The macroscopic properties of the gas, such as velocity, temperature, density, shear stress, pressure, and so on, are obtained by taking the appropriate sampling of microscopic properties of the simulating particles after achieving steady flow.

The micro-perspective and statistical property are two distinct features of the DSMC method. The working process of the DSMC simulation can be summarized as in the following steps:[24] (i) reading the grid data and recording the information about the boundary conditions; (ii) initializing the flow field and calculating the entering number of simulating molecules; (iii) simulating the molecules' motion and interaction with boundary; (iv) indexing all of the simulating molecules; (v) simulating the molecules' probabilistic selection and collision with each other; (vi) sampling the mesh cell and wall information and repeating steps (iii)–(vi) until the flow field reaches a steady state; and (vii) writing out the information about the flow field and wall.

Over the past few decades, the DSMC method has been a predominant predictive tool in rarefied gas flows. However, computational consumption is the main blockage in the extensive application of the DSMC method. Generally speaking, there are two different ways to solve this difficulty when facing massive computation: the first is to improve the DSMC method, such as with MPC algorithm,[25] or asymptotic-preserving (AP) algorithm;[26] the second is to introduce some assistant techniques, such as the efficient parallel technology.[27] In our DSMC code, the parallel technique is employed.

2.2. Validation of the DSMC code

The following numerical simulations are performed by using the DSMC code developed by Liu's team from Shanghai Jiao Tong University, which has been validated with some

typical benchmark cases in our recent researches.[24,26–29] However, to estimate the applicability of the DSMC code for the micro-channel gas flow, the case of a 2D micro-channel (for the geometry of the micro-channel and free stream conditions, please refer to Ref. [1]), in which the simulation data from different researchers are detailed, is used to perform our DSMC simulation to provide the quantitative calculation results for the code validation. For the following DSMC simulations, the computing grid is structured and generated using the commercial software *POINTWISE*, whose mesh number is 64680, which is larger than those used in Refs. [1], [22], and [30]. In addition, the times of sampling, simulating particles in each mesh and time step are all set to be adequate values according to our experience in DSMC simulations, ensuring that the flow fields are always steady. The comparison of DSMC simulation results from our DSMC code and other researchers' is shown in Fig. 1. It is seen that the obtained velocity ratio (a dimensionless parameter defined as the ratio of streamwise velocity of gas, U, to the free stream incoming velocity U_∞) profiles at $x/L = 0.4$ and $x/L = 0.6$ accord well with the existing simulation results in Refs. [1], [22], and [30] except for a slightly constant difference. According to Darbandi,[31] the slight difference could be caused by the computing grid pattern. Therefore, the comparison indicates that our DSMC code can be used for simulating micro-channel gas flow and it has a good simulation accuracy.

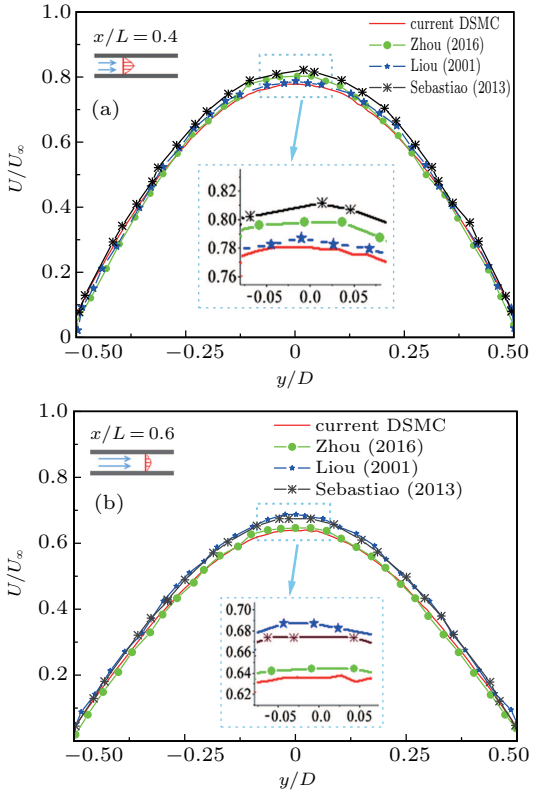


Fig. 1. Velocity ratio profiles along diameter of (a) $x/L = 0.4$ and (b) $x/L = 0.6$ cited from different researchers.

3. Description of simulation cases

According to the published papers, the rectangular micro-channel has been investigated widely, while the circular micro-channel has not received much attention. However, there are many fields using the circular micro-channels. For example, the cooling device (see the left-hand part of Fig. 2) in electronic components commonly use the circular micro-channels to transfer the high heat flux,[32] and the circular micro-channels also exist in other MEMSs, such as micro-pumps, micro-ejectors, micro-valves and micro-mixers.[33] A famous example is that the micro-Pitot tube, which has a circular cross section and plays an important role in the field of high-speed and rarefied plume measurements.[34] Therefore, the circular micro-channel is adopted as a study object in this paper. Considering that both the geometry and flow field of the circular micro-channel are axisymmetric and to reduce the computing cost of DSMC simulations, the 2D circular micro-channel is employed to perform the following numerical simulations, as shown in the right-hand part of Fig. 2.

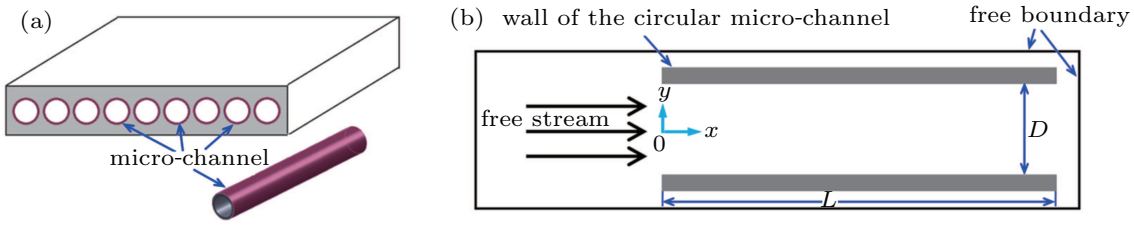


Fig. 2. Schematic diagram of (a) a cooling device with circular micro-channels and (b) DSMC simulation domain.

The internal diameter (D), length (L), and wall thickness of the circular micro-channel are 1.2, 6.0, and 0.1 μm, respectively. The wall temperature is set to be a constant of 300 K. For the DSMC simulation domain, its left-hand side is the inlet condition, where the free stream enters and its right, upper and lower side are the free condition, where the simulating particles move inside or outside freely. The free stream is air consisting of 78% N_2 and 22% O_2 and its inflow parameters such as temperature, pressure, density, and mean free path at different altitudes are listed in Table 1, where the Mach number is a constant of three for different altitudes. Then, the effect of altitude on gas flow in the micro-channel can be obtained by performing the cases in Table 1.

Table 1. Inflow parameters of free stream at different altitudes

Altitude H/km	Mach number (Ma_∞)	Temperature T_∞/K	Pressure P_∞/Pa	Density (ρ_∞)/(kg/m^3)	Mean free path/m
0.5	3	284.9	95461.3	1.167	6.961×10^{-8}
1.0	3	281.7	89876.3	1.112	7.310×10^{-8}
3.0	3	268.7	70121.2	0.909	8.937×10^{-8}
6.0	3	249.2	47217.6	0.660	1.231×10^{-7}
10.0	3	223.3	26499.9	0.414	1.965×10^{-7}
15.0	3	216.6	12111.8	0.195	4.172×10^{-7}

Note that the inflow direction of free stream is parallel to wall of the micro-channel for the cases in Table 1.

As mentioned above, the free stream in practical cases is actually not always parallel to the wall but has a varying inflow direction. Therefore, the effect of free stream inflow direction on gas flow in the micro-channel has to be investigated. First, to indicate the orientation of free stream inflow direction relative to micro-channel wall, the parameter called the angle of attack is proposed and defined as the intersection angle between free stream inflow direction and micro-channel wall. For example, it means that free stream is parallel to the wall when the angle of attack is 0°. Second, the angles of attack of 0°, 3°, 5°, 8°, 12°, and 20° are considered successively to explore the effect of free stream inflow direction on gas flow in the micro-channel. Besides the angle of attack, the free stream with Mach numbers of 2, 3, 4, and 5 are also taken into account to investigate the effect of free stream incoming velocity on gas flow in the micro-channel. It should be noted that the angle of attack is 0° and the altitude is set to be 1.0 km when the simulation cases of different free stream incoming Mach numbers are carried out. Meanwhile, the free stream incoming Mach number and altitude are set to be 3.0 km and 1.0 km, respectively, when the simulation cases of different angles of attack are investigated. In this paper, the incoming Mach number of free stream and angle of attack are denoted by Ma_∞ and a, respectively.

4. Results and discussion

In this section, we present the DSMC simulation results of the supersonic gas flow in a circular micro-channel under different inflow conditions including the free stream at different altitudes, with different incoming Mach numbers and different angles of attack. These three inflow conditions are decoupled and the effect of altitude, incoming Mach number and angle of attack on micro-channel gas flow are investigated, respectively. Because the DSMC is essentially a statistic method, the simulation results of all cases we considered actually reflect the time-averaged flow properties of gas flow in the micro-channel.

4.1. Effect of altitude on micro-channel gas flow

The difference in rarefied degree of gas makes the flow in a micro-channel and in a macro-channel very different. For example, the flow in a macro-channel is continuous and the velocity in the vicinity of wall is regarded as zero,[35] while the slip effect occurs in the vicinity of wall for the flow in a micro-channel due to the increase of rarefied degree of gas. As is well known, the higher the altitude, the more rarefied the gas is. Therefore, it is necessary to explore the effect of the altitude on gas flow in the micro-channel.

The Mach number contours in the flow field for different altitudes are shown in Fig. 3, where the Mach number is normalized by using that of the free flow for each case. It is observed that for all cases, the Mach number contours are symmetrical about the centerline of the micro-channel, and gas flow in the vicinity of the upper wall and of the lower wall are always slowest, while the gas flow at the inlet and at the outlet are usually fast. Moreover, it is also seen that the Mach number contour for the altitudes of 0.5, 1.0, and 3.0 km are very different from that for the altitudes of 6.0, 10.0, and 15.0 km. Specifically, for the altitudes of 0.5, 1.0, and 3.0 km, the shape of the Mach number contour in the micro-channel resembles two flames located at the inlet and outlet, respectively, and the closer to the interior of the 'flame' the contour, the larger the Mach number is. As the altitude increases, length of the 'flame' at the inlet decreases gradually while that at the outlet increases slightly. For the altitudes of 6.0, 10.0, and 15.0 km (see the right part of Fig. 3), the flame-shaped Mach number contours at the inlet are replaced by the arc-shaped Mach number contours there, and the Mach number of gas flow at the inlet is quite low. However, the flame-shaped Mach number contours at the outlet still exist. The reason for this phenomenon is mainly that the rarefied degree of gas increases significantly when the altitude exceeds 6.0 km (see Fig. 4), it is seen that the Knudsen number increases from 0.058 to 0.348 when the altitude varies from 0.5 km to 15.0 km. From this, it can be concluded that the enhancement of rarefied degree will prevent some of the free streams from entering into the micro-channel and consequently the velocity, pressure, and temperature distributions in the micro-channel flowfield change due to the altitude variation. According to Ref. [18], the gas flow in the micro-channel at the altitudes of 6.0, 10.0, and 15.0 km are all in the transition regime (*i.e.*, $0.1 < Kn < 10$), while they are in the slip regime (*i.e.*, $0.001 < Kn < 0.1$) at the altitudes of 0.5, 1.0, and 3.0 km. For the micro-channel gas flow, a significant founding is that the Mach number contours in the transition flow regime and slip flow regime are very different, especially for those around the inlet.

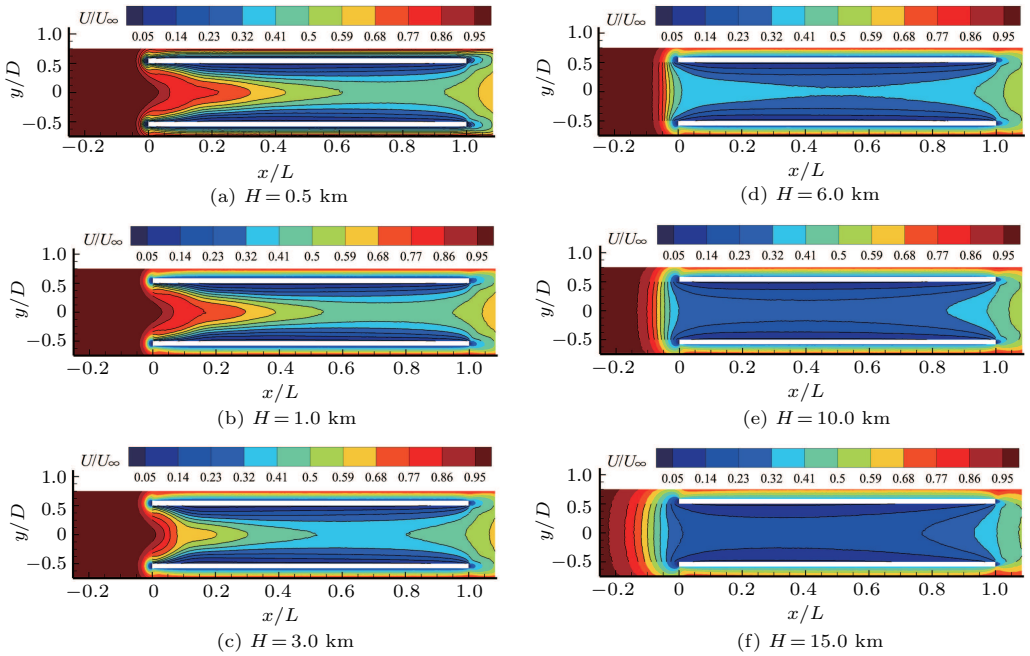


Fig. 3. Comparison of Mach number contours in flow field for different altitudes ($Ma_\infty = 3$, $a = 0°$).

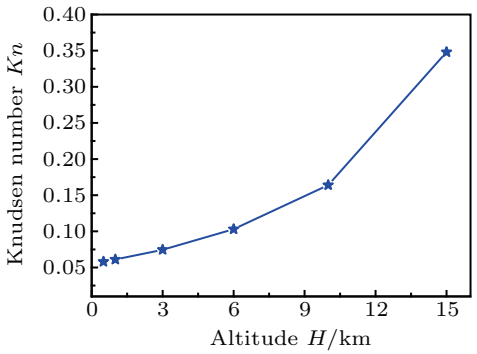


Fig. 4. Variation of Knudsen number with altitude.

Figure 5 shows the pressure contours in the flow field for different altitudes, where the pressure is normalized by using the pressure of the free stream for each altitude. An obvious feature seen from Fig. 5 is that pressure contour in the micro-channel seems to be divided by several straight lines perpendicular to the wall, especially for those located in the middle of the micro-channel. In other words, the pressure contours are approximately stripe-shaped along the diametrical direction. For the pressure around the inlet, it changes remarkably as the altitude increases from 0.5 km to 15 km. For example, the pressure at the inlet is approximately equal to that of the free stream for the altitude of 0.5 km, while it is about 8 times larger than that of the free stream for the altitude of 15.0 km. However, for the pressure around the outlet, it changes slightly for the different altitudes. In addition, another obvious feature that can be found from Fig. 5 is that the high pressure area (HPA), defined as an area in the micro-channel that has a highest pressure on average) gradually moves towards the inlet as the altitude increases and it finally remains at the inlet when the altitude exceeds 10.0 km.

The temperature contours in the flow field for different altitudes are shown in Fig. 6, where the temperature is normalized by using the temperature of the free stream for each altitude. It is observed that the temperature contours for the altitudes of 0.5 km, 1.0 km, and 3.0 km are similar but very different from those for the altitudes of 6.0 km, 10.0 km, and 15.0 km, and the reason for this phenomenon is probably that the flow field varies from slip flow regime to transition flow regime as the altitude increases from 0.5 km to 15.0 km (see the Fig. 4). On the whole, the different temperature contours in the micro-channel usually have a similar shape and the temperature rises gradually from wall to center of the micro-channel along the radial direction for each of the altitudes. For the altitudes of 0.5 km, 1.0 km, and 3.0 km, the high temperature area (HTA), defined as an area in the micro-channel that has a highest temperature on average) gradually moves towards the inlet as altitude increases. However, for the altitudes of 6.0 km, 10.0 km, and 15.0 km, the high temperature area is almost immobile and it is located about at the inlet, and another notable phenomenon is that the temperature contours shrink towards the inlet, which causes the temperature contour to expand about 1.4 times from the outlet towards the inlet as altitude increases.

One interpretation of the physical mechanism for Figs. 3, 5, and 6 is described as follows. The diameter of the circular micro-channel is only 1.2 μm, which is a tiny hole for the incoming free stream. For example, for the free stream, which has a large mean free path of the gas molecule, the mean free path is comparable to the diameter of the micro-channel (for example, the case of $H = 15$ km), a majority of the free stream's molecules probably collide with the wall at the inlet,

so some molecules are blocked from entering into the micro-channel and the molecules which penetrate into the micro-channel are also be decelerated, leading to the low-speed flow of gas near the inlet and the HPA and HTA towards the inlet as the altitude increases. In contrast, when the free stream has a small mean free path of gas molecules (*e.g.*, the case of $H = 0.5$ km), namely the mean free path of gas molecules is very smaller than the diameter of the micro-channel, only a minority of the free stream's molecules collide with the wall at the inlet, so the free stream is affected less by the micro-channel inlet and thus entering into the micro-channel with ease. For this reason, the velocity, pressure, and temperature contours in the micro-channel flowfield change with the altitude (that is, the rarefied degree).

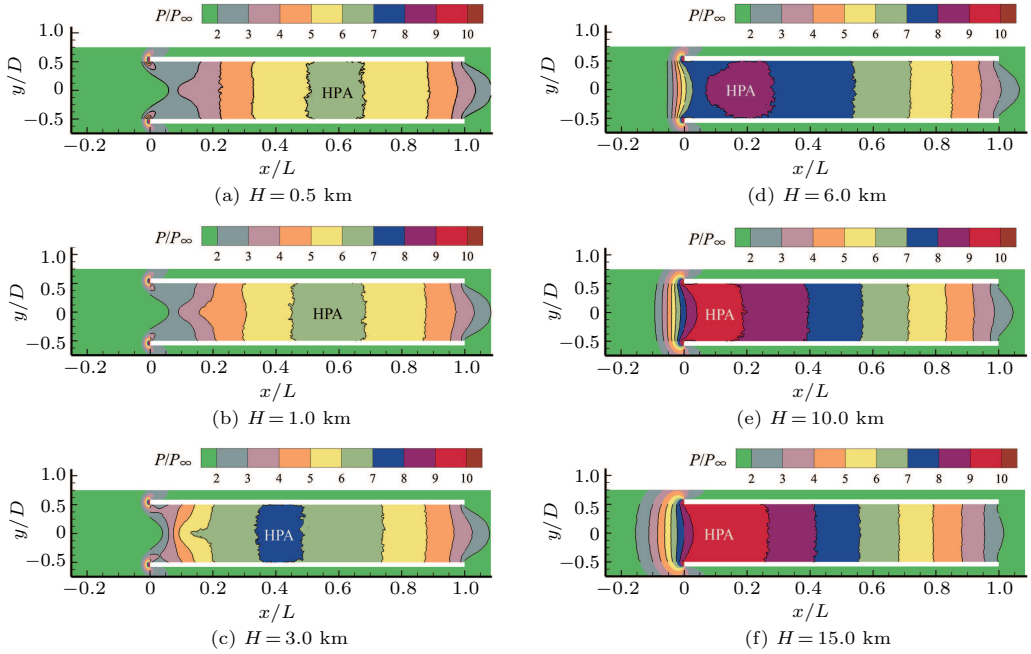


Fig. 5. Comparison of pressure contours in flow field for different altitudes ($Ma_\infty = 3$, $a = 0°$).

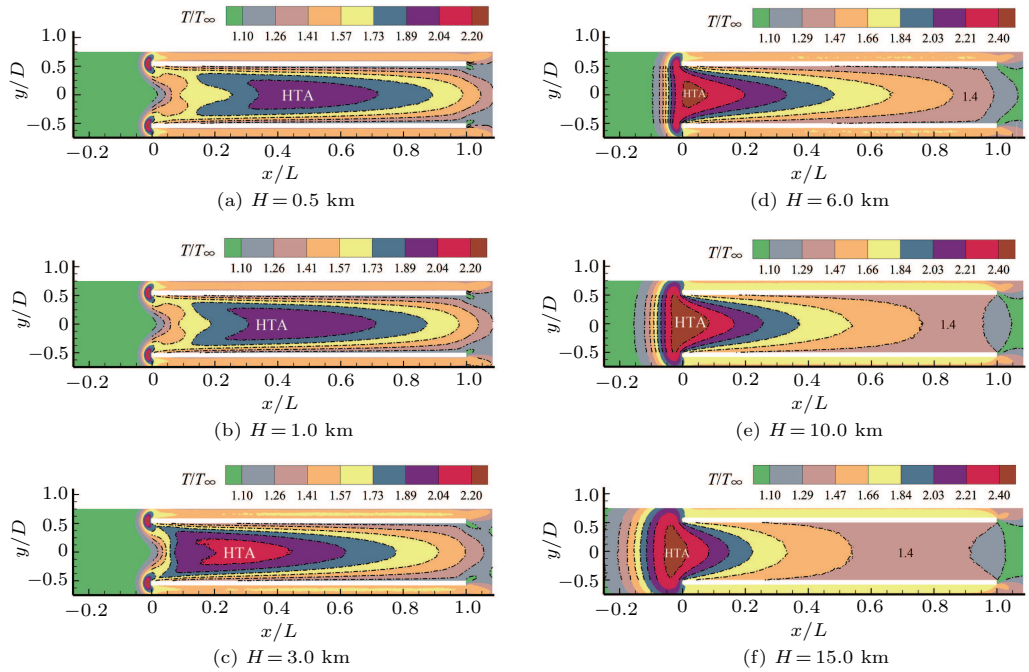


Fig. 6. Comparison of temperature contours in flow field for different altitudes ($Ma_\infty = 3$, $a = 0°$).

The normalized velocity, pressure, and temperature distributions along the centerline of the micro-channel for different altitudes are presented in Fig. 7, where the gray vertical line of $x/L = 0$ is used to indicate the inlet location of the micro-channel. For the altitudes of 0.5, 1.0, and 3.0 km, the normalized velocity, pressure, and temperature at the inlet are approximately 1.0, which means that the velocity, pressure, and temperature at the inlet are equal to those of the free stream. Departing from the inlet,

velocity decreases gradually until the streamwise location of x/L is about 0.7, and then it begins to increase with an increment of about 0.2. The pressure and temperature are both increase sharply at the inlet, then rise with a lower slope before they decrease until the outlet, forming a maximal value in the range of $0.3 < x/L < 0.5$, respectively. For the altitudes of 6.0, 10.0, and 15.0 km, the velocity and pressure at the inlet vary from 0.25 to 0.45 and from 5.5 to 8, respectively, whereas the temperature at the inlet approximately has a constant value of 2.5. Departing from the inlet, the velocity almost remains constant until the streamwise location of x/L is about 0.6, and then it begins to increase with a moderate slope until the outlet. The pressure increases sharply and it has a maximal value of about 0.1 at the streamwise location of x/L, and it then decreases gradually until the outlet. The temperature decreases with the increase of streamwise distance and it finally drops to a value of about 1.2 at the outlet.

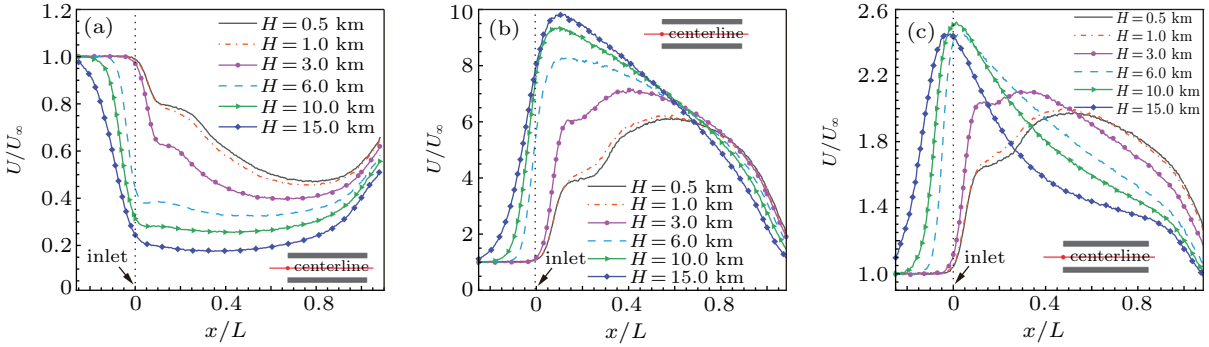


Fig. 7. Profiles of (a) velocity, (b) pressure, and (c) temperature ratios along the centerline of the micro-channel for different altitudes.

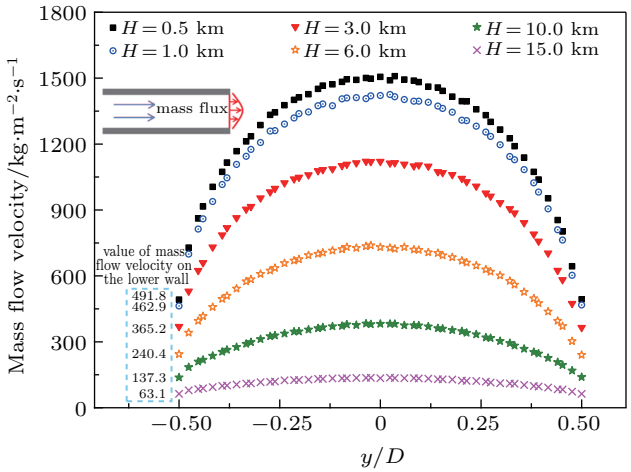


Fig. 8. Profiles of mass flow velocity along diameter of $x/L = 1.0$ for different altitudes ($Ma_\infty = 3$, $a = 0°$).

To reveal the flow efficiency of the free stream passing through the micro-channel, the mass flow velocity defined as the mass flux per unit area per unit time is proposed and calculated along the diameter of $x/L = 1.0$ (*i.e.*, outlet of the micro-channel) for each altitude, and the results are displayed in Fig. 8. It is observed that the profiles of the mass flow velocity for all six different altitudes show a good similarity in shape. That is, each profile of mass flow velocity is symmetric about the central point (*i.e.*, $y/D = 0$) where the mass flow velocity has a maximal value. On the contrary, the mass flow velocity at the wall is lowest. It is also seen that an increase in altitude leads the slope of mass flow velocity distribution to decrease, while the mass flow velocities at the same position for different altitudes decrease greatly. For example, the variation of mass flow velocity distribution is quite slight for the altitude of 15.0 km while it is violent for the altitude of 0.5 km and moreover, the mass flow velocities on the wall are 63.1 kg/(m^2·s) and 491.8 kg/(m^2·s) for the altitudes of 15.0 km and 0.5 km, respectively. Therefore, an important conclusion is that the mass flux of the free stream passing through the micro-channel decreases greatly as the altitude increases. There are two reasons for this phenomenon: first, the gas density is lower at a higher altitude; and second, the rarefaction effect becomes more dominant at a high altitude and it would partly prevent the free stream from entering into the micro-channel.

To provide an in-depth understanding of the high temperature area in the micro-channel, the high temperature area for each case is visualized by extracting its isoline and labeling its minimal and maximal values. Figure 9 shows the evolution of the high temperature area as altitude increases. It should be noted that its minimum temperature is set to be 510 K for an altitude of 15.0 km and it is set to be 550 K for the remaining altitudes. It can be seen that as the altitude increases, the high temperature area moves towards the inlet and it approximately remains at the inlet when the altitude exceeds 6.0 km, and the high temperature area shrinks gradually in the streamwise, while it expands in the spanwise direction. As a result, the shape of the high temperature area is like a stopper blocking the inlet of the micro-channel for each of the altitudes of 6.0, 10.0, and 15.0 km. In addition, the peak temperature of the high temperature area varies slightly (*i.e.*, 562 → 561 → 565) from 0.5 km to 3.0 km, whereas it increases remarkably (*i.e.*, 565 → 612) from 3.0 km to 6.0 km, then it begins to come down and it is only 531 K for the altitude of 15.0 km.

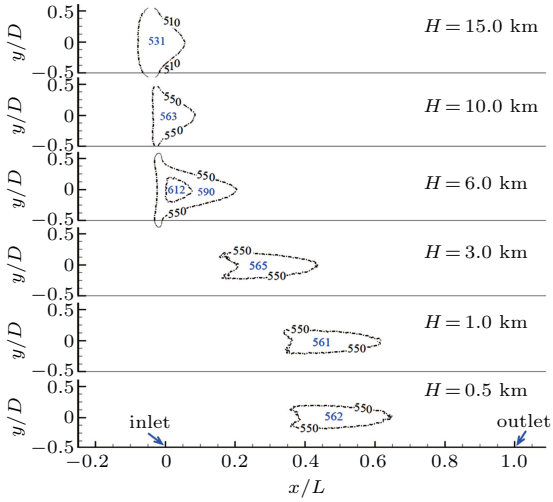


Fig. 9. Evolutions of high temperature area in the micro-channel for different altitudes (temperature unit: K; $Ma_\infty = 3$, $a = 0°$).

4.2. Effect of incoming Mach number on micro-channel gas flow

The free stream incoming Mach number is an important factor affecting the micro-channel flow because it has a great influence on the flow structure and heat transfer performance of the flow field. In addition, the free stream with a high supersonic speed has been investigated rarely. Figure 10 shows the comparison of the Mach number contours in the flow field for the free stream incoming Mach numbers of 2.0, 3.0, 4.0, and 5.0, where the Mach number is normalized by using that of the free stream for each case. It is observed that, for all cases, the Mach number contours are symmetrical about the centerline of the micro-channel and the gas flow in the vicinity of wall is slowest, whereas the gas flow at the inlet and outlet are usually fast. For the free stream incoming Mach number of 2.0, it is seen that the free stream is decelerated before it reaches the inlet and its normalized Mach number is only about 0.33 at the inlet, and then the gas flow will be accelerated gradually after it has passed through the streamwise location of $x/L = 0.6$. On the whole, the gas flow in the micro-channel is quite slow for the free stream incoming Mach number of 2.0. For the free stream incoming Mach numbers of 3.0, 4.0, and 5.0, it is observed that the free stream can penetrate into the micro-channel and it has a farther distance from the inlet for a larger incoming Mach number, which results in a fast gas flow in the micro-channel. That is, increasing the free stream incoming Mach number can accelerate the gas flow and therefore a significant finding is that the rarefaction effect will become very dominant if the free stream incoming Mach number is low, and then free stream will be decelerated greatly before it reaches the inlet. For the geometry of the current micro-channel and the simulation conditions, the rarefaction effect will become quite serious when free stream incoming Mach number decreases to 2.0.

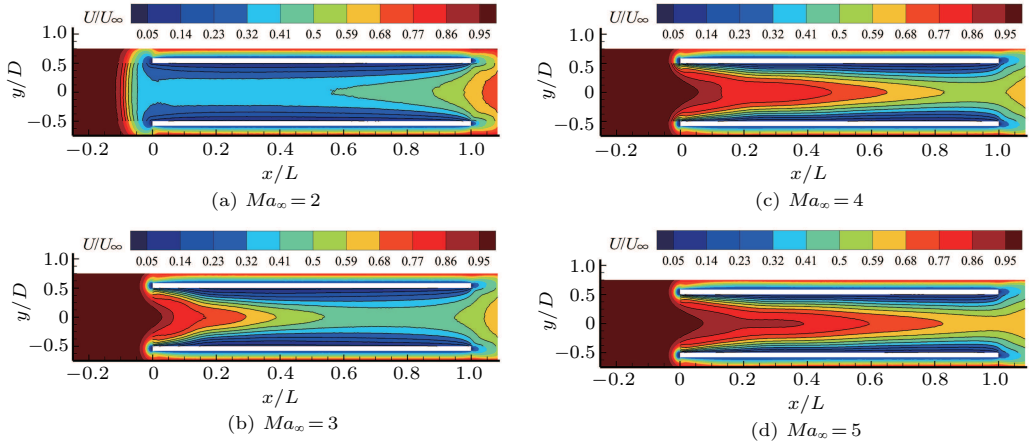


Fig. 10. Comparison of Mach number contours in flow field for different free stream incoming Mach numbers ($a = 0°$, $H = 1$ km).

The pressure contours in the flow field for different free stream incoming Mach numbers are shown in Fig. 11, where the pressure is normalized using that of the free stream for each case. From Fig. 11, it is first observed that the high pressure area in the micro-channel moves towards the outlet as incoming Mach number increases and finally reaches the outlet for the incoming Mach number of 5.0. Second, it observed that the shape of the pressure contour in the micro-channel is changed gradually as incoming Mach number increases. Specifically, the shape change of the pressure contour starts from the inlet because the flow field around the inlet is first affected by the free stream and then it spreads across the entire interior space of the micro-channel; for example, the stripe-shaped pressure contours are nearly completely destroyed for the case of $Ma_\infty = 5$.

The temperature contours in the flow field for different free stream incoming Mach numbers are shown in Fig. 12, where the temperature is normalized by using that of the free stream for each case. With the increase of free stream incoming Mach number, the temperature in the micro-channel rises obviously, while the high temperature area is driven away from the inlet. Specifically, the high temperature area is located at the inlet for the incoming Mach number of 2.0 and it moves to the central position for the incoming Mach number of 3.0, and for the incoming Mach numbers of 4.0 and 5.0, the high temperature area not

only reaches the outlet but also occupies quite a large domain, and another notable feature is that a small peak temperature zone, which is close to the outlet, appears within the high temperature area.

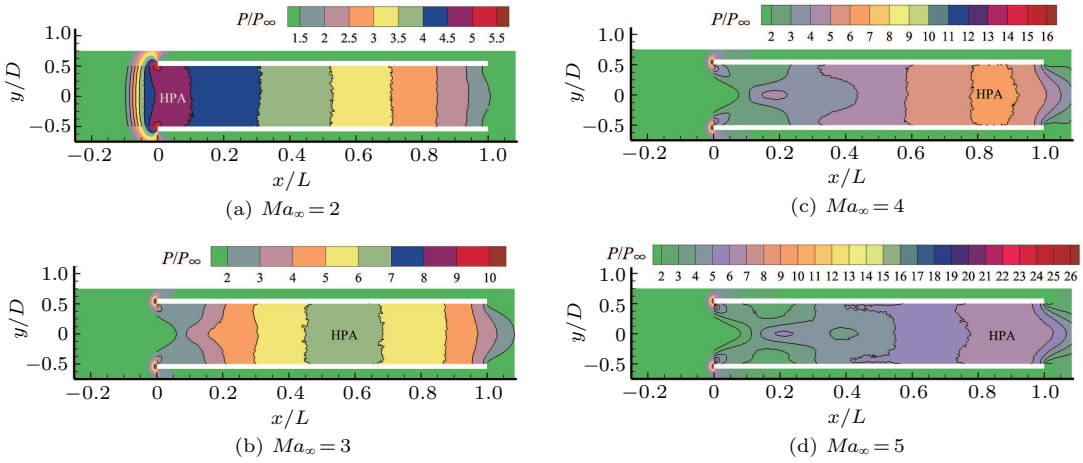


Fig. 11. Comparison of pressure contours in flow field for different free stream incoming Mach numbers ($a = 0°$, $H = 1$ km).

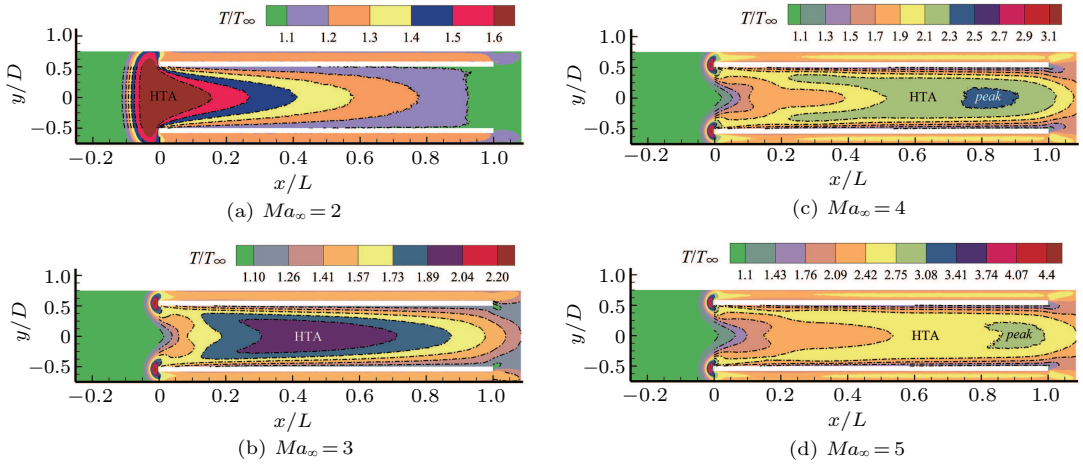


Fig. 12. Comparison of temperature contours in flow field for different free stream incoming Mach numbers ($a = 0°$, $H = 1$ km).

The physical mechanism for Figs. 10–12 is probably that the free stream with a larger incoming velocity is able to penetrate more deeply into the micro-channel, pushing the HPA and HTA to the outlet, while they are expanded and their values are raised.

Figure 13 displays the normalized velocity, pressure, and temperature distributions along the centerline of the micro-channel for different free stream incoming Mach numbers, where the gray vertical line of $x/L = 0$ is used to indicate the inlet location of the micro-channel. For incoming Mach numbers of 3.0, 4.0, and 5.0, it is seen that the velocity distributions show the same variation trend and share almost an identical velocity at the outlet, and the velocity decreases as streamwise distance increases. However, for the incoming Mach number of 2.0, the velocity distribution varies slightly before the streamwise location of about 0.6 and it then increases gradually until the outlet.

For the pressure and temperature distributions, both of them show the same change regulation for each incoming Mach number. Specifically, with the increase of streamwise distance, the pressure and temperature decrease monotonically for the incoming Mach number of 2.0, while they increase rapidly before they decrease until the outlet for the incoming Mach number of 3.0, forming a curve that is approximately symmetric about the $x/L = 0.55$ and $x/L = 0.45$, respectively. For the incoming Mach numbers of 4.0 and 5.0, the pressure and temperature increase sharply at the inlet, then decrease with a small range and increase again before they decrease until the outlet, forming two local maxima at the streamwise locations of about 0.2 and 0.95, respectively.

The mass flow velocity is calculated along the diameter of $x/L = 1.0$ and the results for different free stream incoming Mach numbers are displayed in Fig. 14. It is observed that the profiles of the mass flow velocity for these four incoming Mach numbers show a good similarity in shape. Specifically, each profile of the mass flow velocity is symmetric about the central point (*i.e.*, $y/D = 0$), where the mass flow velocity has a maximal value, whereas it is minimum at the wall. It is also

seen that an increase in incoming Mach number not only leads to a large increase in the slope of the mass flow velocity distribution but also results in a great increase in the mass flow velocity. For example, the profile of the mass flow velocity for the incoming Mach number of 5.0 is more pointed than the profiles of the mass flow velocity for the incoming Mach numbers of 2.0, 3.0, and 4.0, and the mass flow velocities on the wall for the incoming Mach numbers of 2.0, 3.0, 4.0, and 5.0 are 220.8, 462.9, 612.1, and 710.3 kg/(m^2·s), respectively. That is, the mass flux of the free stream passing through the micro-channel increases significantly as the incoming Mach number increases.

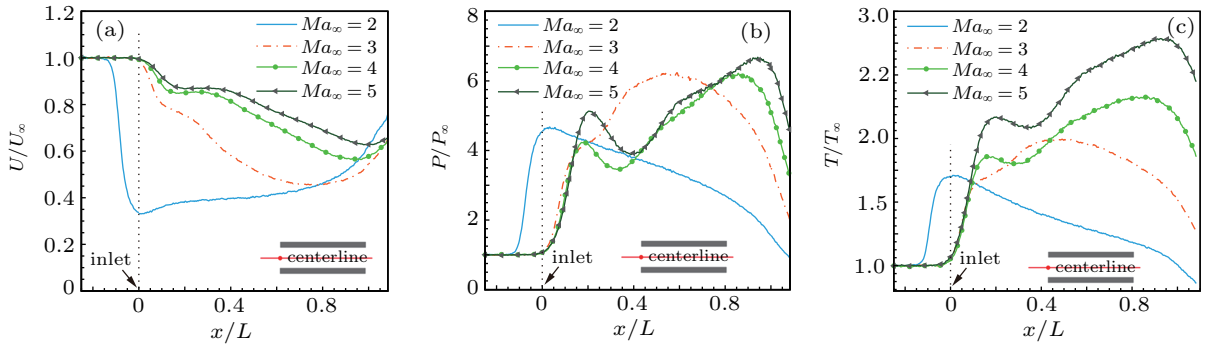


Fig. 13. Profiles of (a) velocity, (b) pressure, and (c) temperature ratios along centerline of the micro-channel for different free stream incoming Mach numbers.

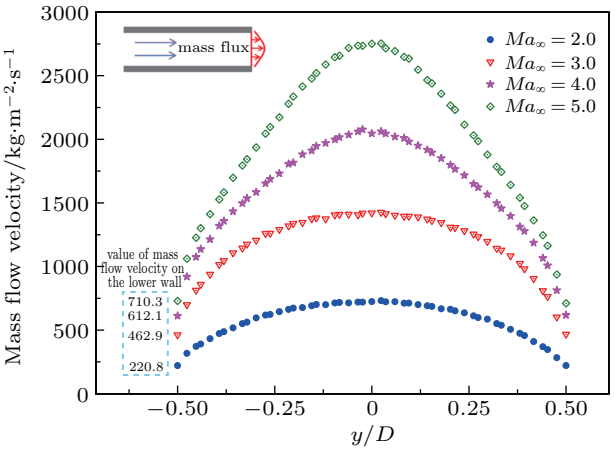


Fig. 14. Profiles of mass flow velocity along diameter of $x/L = 1.0$ for different free stream incoming Mach numbers ($a = 0°$, $H = 1$ km).

Figure 15 shows the visualized high temperature area in the micro-channel for different free stream incoming Mach numbers. And note that their minimum temperatures are set to be 460, 550, 600, and 730 K for the Mach numbers of 2.0, 3.0, 4.0, and 5.0, respectively. It is observed that the high temperature area moves towards the outlet as incoming Mach number increases and it will remain at the outlet when the free stream incoming Mach number exceeds 4.0, while both its shape and peak temperature are changed greatly as incoming Mach number increases. For example, for the free stream incoming Mach numbers of 4.0 and 5.0, high temperature areas each occupy most of the space in the micro-channel and their peak temperatures are about 658 K and 782 K, respectively. However, for the free stream incoming Mach numbers of 2.0 and 3.0, the high temperature areas each only hold a small space in the micro-channel and their peak temperatures are 480 K and 561 K, respectively. Note that the shapes of the high temperature areas seem to be alike for the free stream incoming Mach numbers of 4.0 and 5.0. According to Darbandi and Roohi,[5] compressibility and rarefaction effect are two key factors determining the gas flow in the micro-channel. For the free streams at the same altitude, therefore, it can be concluded that the compressibility effect will gradually become more dominant than the rarefaction effect as the incoming Mach number increases, and then the gas flow in the micro-channel is determined mainly by the compressibility of the free stream, which is equivalent to the free stream incoming Mach number, such as in the cases of $Ma_\infty = 4.0$ and $Ma_\infty = 5.0$.

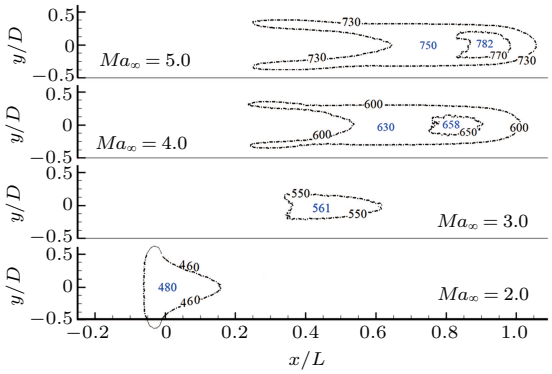


Fig. 15. Evolutions of high temperature area in micro-channel for different free stream incoming Mach numbers (temperature unit: K; $a = 0°$, $H = 1$ km).

4.3. Effect of angle of attack on micro-channel gas flow

The free stream in some practical cases is not always parallel to the wall of the micro-channel but it tends to have a varying inflow direction. However, there has been little numerical work on the free stream inflow direction despite the fact that it has an important effect on the gas flow in the micro-channel. In this paper, the free stream inflow direction is represented by the angle of attack, and the angles of attack of 0°, 3°, 5°, 8°, 12°, and 20° are considered in this subsection to

explore the influence of the free stream inflow direction on the gas flow in the micro-channel.

Figure 16 shows the Mach number contours in the flow field for different angles of attack, where the white arrows in each case indicate the free stream inflow direction. Note that the presented Mach number is normalized by using that of the free stream for each case. As the angle of attack increases, it is observed that the Mach number contours are gradually no longer symmetrical about the centerline of the micro-channel, especially for the left micro-channel flow field. Another notable feature is that the gas flow in the micro-channel becomes slower as the angle of attack increases, and the reason is attributed to the impediment effect of the upper wall at the inlet. In other words, the free stream obtains a greater opportunity of impacting the upper wall at the inlet as the angle of attack increases, which results in a deceleration action of gas when it passes through the inlet. In addition, the downstream boundary layer of the lower wall becomes thicker for a larger angle of attack. Therefore, increasing the angle of attack will decelerate the flow of gas at the inlet and thicken the downstream boundary layer of the lower wall.

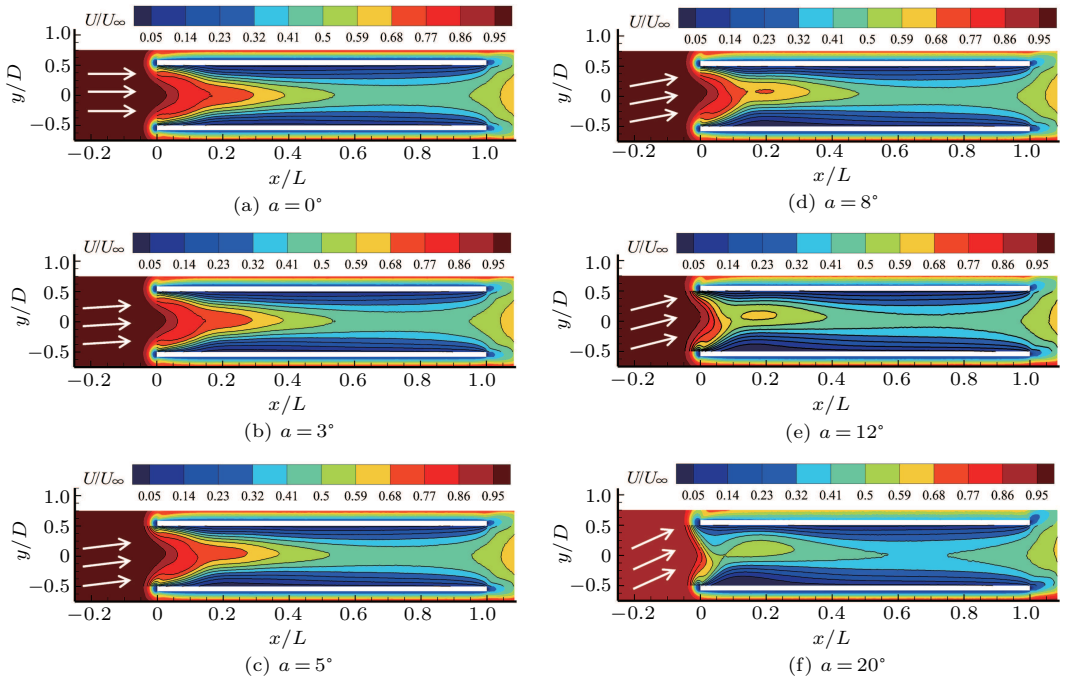


Fig. 16. Comparison of Mach number contours in flow field for different angles of attack ($Ma_\infty = 3$, $H = 1$ km).

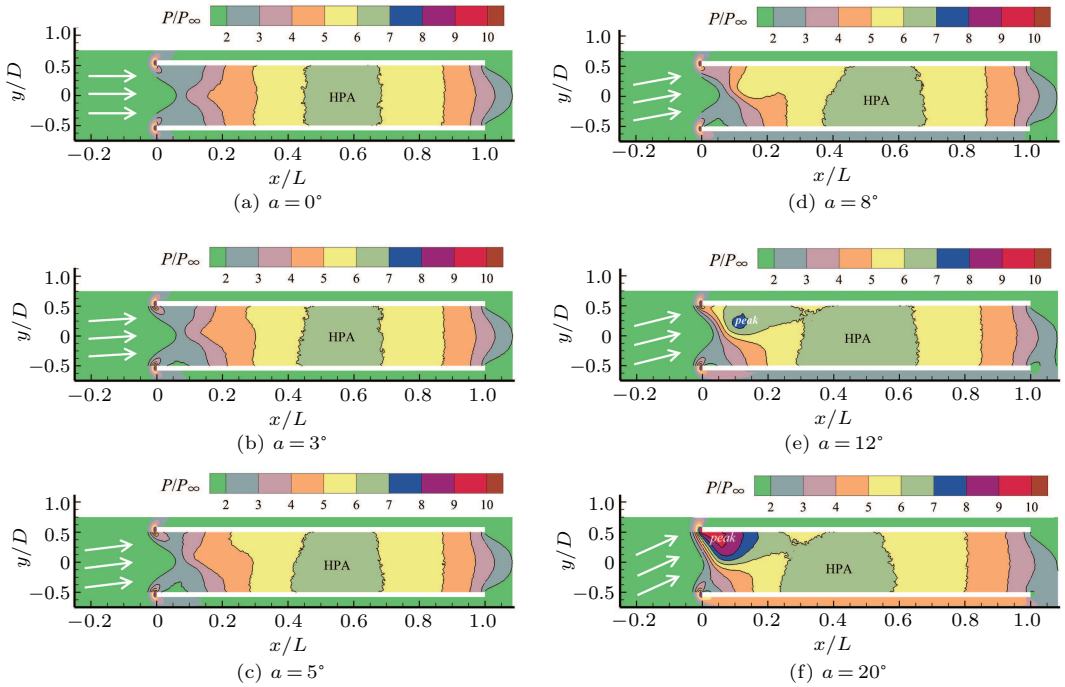


Fig. 17. Comparison of pressure contours in flow field for different angles of attack ($Ma_\infty = 3$, $H = 1$ km).

The pressure contours in the flow field for different angles of attack are shown in Fig. 17, where the pressure is normalized by using that of the free stream and the white arrows in each case indicate the free stream inflow direction. An obvious feature can be seen from Fig. 17 is that the angle of attack mainly affects the pressure contours in the entrance part of the micro-channel flow field and, consequently, the whole micro-channel flow field can be divided into three distinct parts. The first part is about in the range of $0 < x/L < 0.3$, in which the pressure contours are affected greatly by the angle of attack. For example, the symmetric character of pressure contours about the centerline of the micro-channel is destroyed completely in this range and moreover a small pressure peak zone appears near the upper wall approaching to the inlet when the angle of attack is large (*e.g.*, 12° and 20°). The second part is about in the range of $0.3 < x/L < 0.7$, and it is actually almost occupied by the high pressure area. It is observed that the high pressure area expands gradually as the angle of attack increases, while it moves slightly towards the inlet. The third part is the remaining region of the micro-channel, namely the range of $x/L > 0.7$, it is seen that the pressure contours in this range is almost invariable as the angle of attack increases.

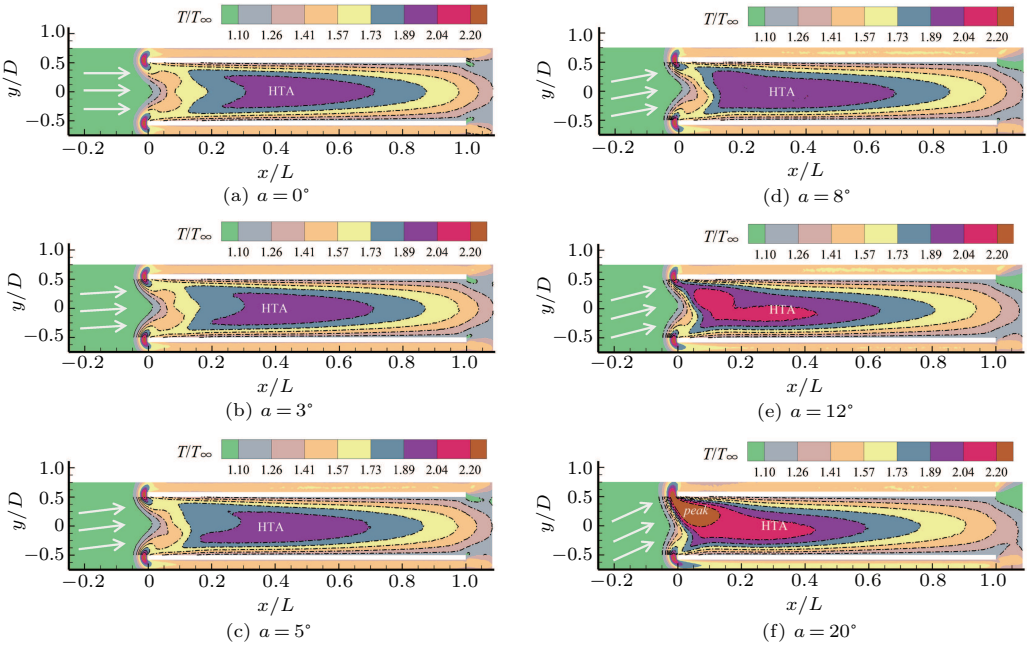


Fig. 18. Comparison of temperature contours in flow field for different angles of attack ($Ma_\infty = 3$, $H = 1$ km).

The normalized temperature contours in the flow field for different angles of attack are shown in Fig. 18, where the white arrows in each case indicate the inflow direction of the free stream. Like the variation of pressure contours, the angle of attack mainly affects the temperature contours in the entrance part of the micro-channel flow field. With the increase of angle of attack, it is seen that the high temperature area expands gradually, while it moves towards the inlet. For the angle of attack of 12°, it is found that a smaller area with higher temperature is generated within the high temperature area and for the angle of attack of 20°, a small peak temperature zone appears at the upper wall approaching to the inlet due to the drastic collision between the free stream and the upper wall. For the exit part of the micro-channel flow field (*i.e.*, $x/L > 0.7$), it seems that temperature contours are almost unaffected by the angles of attack.

The physical mechanism for Figs. 16–18 can be illuminated as follows. With the increase of the angle of attack, more gas molecules from the free stream, which have the supersonic speed velocity, are able to collide with the micro-channel inner wall near the inlet and probably accumulate themselves on the inner wall, result in deceleration of the gas molecules entering into the micro-channel, and the enhancement of pressure and temperature of the gas near the collision location. Consequently, the flow speed of the gas in the micro-channel gradually decreases as the angle of attack increases, while both the HPA and HTA move towards the collision location.

The normalized velocity, pressure, and temperature distributions along the centerline of the micro-channel for different angles of attack are presented in Fig. 19, where the gray vertical line of $x/L = 0$ is used to indicate the inlet location of the micro-channel. For these six different angles of attack, it is observed that the velocity distributions show the same variation trend and share almost an identical velocity at the outlet, and so do the pressure and temperature distributions. Actually, the velocity, pressure, and temperature distributions in the range of $x/L > 0.5$ are almost the same for different angles of attack, but they are very different in the range of $0 < x/L < 0.5$, and the reason is that the angle of attack mainly affects the gas flow in the entrance part of the micro-channel, which accords

with the analysis above. Specifically, the velocity in the range of $0 < x/L < 0.5$ decreases whereas the pressure and temperature in this range increase as the angle of attack increases, and there is a oscillation region for each of velocity, pressure, and temperature distribution at the normalized streamwise location of about 0.15 for a large angle of attack (*e.g.*, 8°, 12°, and 20°), respectively.

The mass flow velocity is calculated along the diameter of $x/L = 1.0$, and the results for different angles of attack are displayed in Fig. 20. It is seen that the profiles of the mass flow velocity for these six angles of attack show that they in very good consistence in shape, what is more, they do not show a significant difference in mass flow velocity with the increase of angle of attack. That is, an increase in angle of attack only leads to a slight decrease in mass flow velocity. From Fig. 20, a notable feature that can be found is that the mass flow velocity at the upper and lower wall (*i.e.*, $y/D = 0.5$ and $y/D = -0.5$) for each angle of attack are slightly different due to the asymmetrical gas flow in the micro-channel which is caused by the angle of attack.

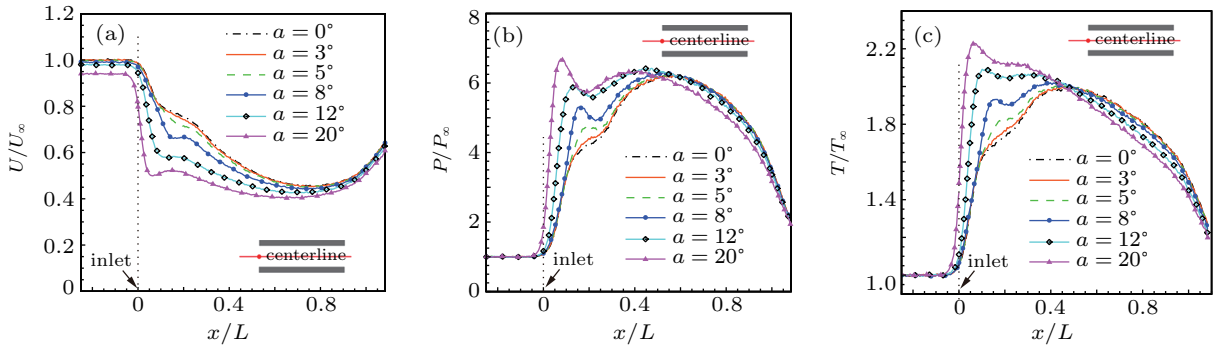


Fig. 19. Profiles of (a) velocity, (b) pressure, and (c) temperature ratios along central line of micro-channel for different angles of attack.

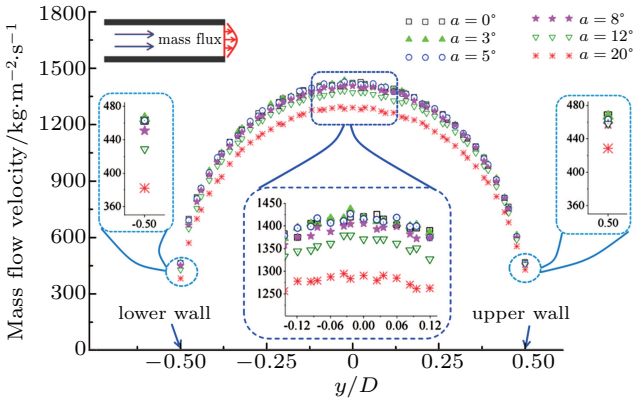


Fig. 20. Profiles of mass flow velocity along diameter of $x/L = 1.0$ for different angles of attack ($Ma_\infty = 3$, $H = 1$ km).

Figure 21 shows the visualized high temperature areas in the micro-channel for different angles of attack. It is obvious that the high temperature area is greatly affected by the angle of attack; for example, the high temperature area expands greatly, while its peak temperature increases significantly as the angle of attack increases. The high temperature area even expands to the inlet when the angle of attack is larger than 12° and the peak temperatures of the high temperature area are 561, 563, 567, 577, 611, and 690 K for the angles of attack of 0°, 3°, 5°, 8°, 12°, and 20°, respectively. In addition, a noteworthy feature that can be seen from Fig. 21 is that the position of the peak temperature moves from the center to the top left corner of the high temperature area as the angle of attack increases from 0° to 20°. The reason for this phenomenon is that the free stream will directly strike the upper wall under the condition of a large angle of attack (*e.g.* 12° and 20°) and the greater the angle of attack, the more drastic the strike is, resulting in the peak temperature appearing near the strike point.In addition to the peak temperature moving, it is seen that the increase in angle of attack also leads to an increase in the temperature in the center of the high temperature area.

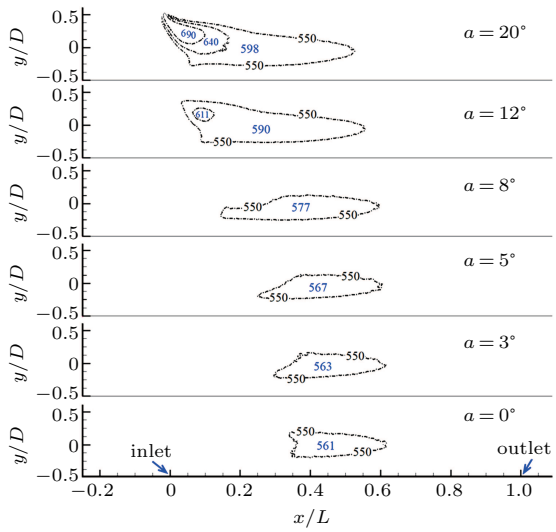


Fig. 21. Evolutions of high temperature area in micro-channel for different angles of attack (temperature unit: K; $Ma_\infty = 3$, $H = 1$ km).

5. Conclusions

In this paper, a DSMC method is used to investigate the primary properties of the supersonic gas flow in a circular micro-channel by considering different inflow conditions. For each inflow condition that we considered, the velocity, pressure, and temperature contour of the micro-channel flow field,

the velocity, pressure, and temperature distributions along the centerline of the micro-channel, the mass flow velocity of the outlet as well as the evolution of high temperature area in the micro-channel flow field are all shown and analyzed in detail, and we observe that the altitude, Mach number, and angle of attack greatly affect the flow properties of the supersonic gas passing through the micro-channel. Summarizing this paper, the following conclusions can be drawn:

(I) With the increase of altitude, the free stream is gradually decelerated before it reaches the inlet and it will be partly prevented from entering into the micro-channel due to the increase of rarefaction effects. Consequently, the mass flow velocity of the outlet decreases greatly as altitude increases. In addition, an increase in altitude drives both the high pressure and high temperature areas to move towards the inlet and both of them finally remain at the inlet when the altitude exceeds 6.0 km. Then, the shape of the high temperature area is like a stopper blocking the inlet of the micro-channel.

(II) The gas flow in the micro-channel is accelerated and both the pressure and temperature in the micro-channel flow field rise as the incoming Mach number increases. Meanwhile, the high pressure and high temperature area move towards the outlet and both of them finally remain at the outlet. Moreover, mass flux of the free stream passing through the micro-channel increases greatly as free stream incoming Mach number increases. A notable finding is that the rarefaction effects become dominant when the free stream incoming Mach number drops to 2. In other words, the free stream with a larger incoming velocity is able to reduce the influence of the rarefaction effects on the gas flow in the micro-channel.

(III) The velocity, pressure, and temperature in the entrance part of the micro-channel flow field are affected significantly by the angle of attack while those in the exit part are almost not affected, so the mass flow velocity of the outlet decreases slightly as the angle of attack increases. An increase in angle of attack decelerates the gas flow but increases the pressure and temperature in the micro-channel. Under the condition of a large angle of attack (*e.g.*, 12° and 20°), the high temperature area expands to the inlet and its peak temperature rises greatly due to the drastic collision between the free stream and the wall approaching the inlet.

Acknowledgment

The authors thank Prof. H Liu's team of Shanghai Jiao Tong University for providing the DSMC code for this research.

References

[1] Zhou H, Cai G B and He B J 2016 *Appl. Therm. Eng.* **109** 217
[2] Fang Y C and Liou W W 2002 *J. Heat Transfer* **124** 338
[3] Ho C M and Tai Y C 1998 *Ann. Rev. Fluid Mech.* **30** 579
[4] Wang M R and Li Z X 2004 *Int. J. Heat Fluid Flow* **25** 975
[5] Darbandi M and Roohi E 2011 *Int. Commun. Heat Mass* **38** 1443
[6] Sebastiao I B and Santos W F 2014 *Appl. Therm. Eng.* **62** 58
[7] Cercignani C 1987 *The Boltzmann Equation and Its Applications.* (Springer-Verlag New York Inc.) p. 359
[8] Akhlaghia H and Roohi E 2016 *Comput. Fluids* **127** 78
[9] Bird G A 1976 *Molecular Gas Dynamics* (Oxford: Clarendon Press)
[10] Bird G A 1994 *Molecular Gas Dynamics and the Direct Simulation of Gas Flows* (Oxford: Clarendon Press)
[11] Zhang Y B 2018 *Int. J. Heat Mass Transfer* **125** 681
[12] Taassob A, Kamali R and Bordbar A 2018 *Vacuum* **151** 197
[13] Yao Z H, Zhang X W and Xue X B 2011 *Appl. Math. Model* **35** 2016
[14] Torre F L, Kenjereš S, Moerel J L and Kleijn C R 2011 *Comput. Fluids* **49** 312
[15] San O, Bayraktar I and Bayraktar T 2009 *Int. Commun. Heat Mass* **36** 402
[16] Wang H T, Chen Z H and Gao J G 2016 *Appl. Therm. Eng.* **107** 870
[17] Taheri P and Struchtrup H 2010 *Physica A* **389** 3069
[18] White C, Borg M K, Scanlon T J and Reese J M 2013 *Comput. Fluids* **71** 261
[19] Zhen C E, Hong Z C, Lin Y J and Hong N T 2007 *Numer. Heat Transfer Part. A* **52** 239
[20] Gatsonis N, Al-Kouz W and Chamberlin R 2010 *Phys. Fluids* **22** 032001
[21] Ejtehadi O, Roohi E and Esfahani J A 2012 *Int. Commun. Heat Mass* **39** 439
[22] Liou W W and Fang Y C 2001 *J. Microelectromech. S.* **10** 274
[23] Cercignani C 1975 *Theory and Application Of The Boltzmann Equation* (Edinburgh Scottish Academic Press)
[24] Guo G M, Liu H and Zhang B 2017 *Acta Astronaut.* **132** 256
[25] Schwartzentruber T E and Boyd I D 2006 *J. Comput. Phys.* **215** 402
[26] Ren W, Liu H and Jin S 2014 *J. Comput. Phys.* **276** 380
[27] Guo G M and Luo Q 2018 *Int. J. Mech. Sci.* **148** 496
[28] Guo G M, Liu H and Zhang B 2016 *Appl. Opt.* **55** 4741
[29] Zhang B, Liu H and Jin S 2016 *J. Comput. Phys.* **305** 575
[30] Sebastiao I B and Santos W F 2013 *Appl. Therm. Eng.* **52** 566
[31] Darbandi M and Roohi E 2011 *Microfluid Nanofluid* **10** 321
[32] Sharath P, Rao C, Rahman M M and Soliman H M 2006 *Numer. Heat Tranf. A* **49** 635
[33] Aniskin V M, Mironov S G, Maslov A A and Tsyryulnikov I S 2015 *Microfluid Nanofluid* **19** 621
[34] Aniskin V, Mironov S and Maslov A 2013 *Microfluid Nanofluid* **14** 605
[35] Wang X 2006 *Fundamental of Gas Dynamics* (Xi'an: Northwest Industrial University Press)